The Crystal Structure of the Low-Temperature $Au_{80-v}Cu_vSn_{20}$ Phase

O. B. Karlsen, A. Kjekshus,* C. Rømming and E. Røst

Department of Chemistry, University of Oslo, Blindern, N-0315 Oslo 3, Norway

Karlsen, O. B., Kjekshus, A., Rømming, C. and Røst, E., 1992. The Crystal Structure of the Low-Temperature $Au_{80-v}Cu_vSn_{20}$ Phase. – Acta Chem. Scand. 46: 1076–1082.

The crystal structure of the low-temperature $Au_{80-v}Cu_vSn_{20}$ phase has been determined by direct methods. Low-temperature $Au_{80-v}Cu_vSn_{20}$ takes the β-Mn-type structure (space group $P4_132$). For $v = 45$: $a = 676.2(2)$ pm, Cu in 8c with $x = 0.0629(3)$ and 0.583 Au + 0.083 Cu + 0.333 Sn statistically distributed in 12d with $y = 0.2016(1)$. For $v = 60$: $a = 666.2(2)$ pm, Cu in 8c with $x = 0.0643(2)$ and 0.333 Au + 0.333 Cu + 0.333 Sn statistically distributed in 12d with $y = 0.2022(1)$. Refinements in terms of the lower symmetric, $AlAu_4$-type structure (space group $P2_13$) gave only insignificant improvements in reliability factors, and fractional coordinates which deviated by less than two standard deviations from the conditions pertinent to the β-Mn type. Different descriptions of the β-Mn-type structure are considered, and their advantages are briefly discussed. LT $Au_{80-v}Cu_vSn_{20}$ is considered in relation to established features of the β-Mn- and $AlAu_4$-type structures.

The present authors have previously reported[1–3] on the phase relations in the Au–Cu–Sn system and the crystal structure of one (explicitly AuCuSn, also labelled C in Refs. 1 and 2) of the three genuine ternary phases. This paper concerns the crystal structure of phase B. The composition of phase B is approximately described by the formula $Au_{80-v}Cu_vSn_{20}$ with $42 \leq v \leq 69$ at 360 °C, where the variation in Sn content is less than 3 atom %. (For further details about the homogeneity range see Ref. 2.) Phase B has the character of a low-temperature phase relative to A, and since the latter also obeys the same formula, phase B will be referred to as low-temperature (LT) $Au_{80-v}Cu_vSn_{20}$ whenever complete specification is needed.

Sample provenance

Samples with nominal compositions $Au_{35}Cu_{45}Sn_{20}$ and $Au_{20}Cu_{60}Sn_{20}$ were prepared by melting together weighed amounts of the (>99.9 % pure)[1,2] elements in sealed, evacuated silica-glass tubes. After quenching into ice water the samples were annealed for about one week at 360 °C. Cautious crushing of the coarse-grained samples thus obtained gave (according to examination by the Weissenberg technique) suitable single-crystal fragments for the structure determination.

X-Ray data and structure determination

Crystal and experimental data are given in Table 1. Unit cell dimensions were calculated from diffractometer setting angles for 25 ($v = 45$) or 15 ($v = 60$) reflections with $25 < 2\theta < 37°$ ($v = 45$) or $19 < 2\theta < 31.5°$ ($v = 60$). The numerical values for the lattice parameter, a, in Table 1 are in conformity with the compositional variation of a for $Au_{80-v}Cu_vSn_{20}$ in Ref. 2, and the nominal composition parameters $v = 45$ and 60 are consequently regarded as representative of the real composition of the crystals. Intensities for both crystals were recorded for an octant of reciprocal space and corrected for Lorentz and polarization effects. The structure of $v = 60$ was determined by direct methods,[4] and refined by least-squares calculations[5] using isotropic thermal parameters. The results show that the position 8c is occupied solely by Cu and that all Au and Sn plus the excess of Cu are statistically distributed over the position 12d. The data for both crystals were corrected for absorption through empirical methods[6] (minimum and maximum absorption corrections were 0.85 and 1.37 for $v = 45$ and correspondingly 0.91 and 1.57 for $v = 60$), and the intensities of equivalent reflections were averaged. The positional and anisotropic thermal parameters were finally refined by least-squares calculations. The occupation factor for the atoms in the mixed Au, Cu and Sn position were kept constant at the composition value for the crystal in question during the refinements. (According to pycknometric density[1] there are 20 atoms in the unit cell, which give $Au_7Cu_9Sn_4$ and $Au_4Cu_{12}Sn_4$ for $v = 45$ and 60, respectively, implying that, respectively, 7 Au + 1 Cu + 4 Sn and 4 Au + 4 Cu + 4 Sn are accommodated in the mixed position.)

Refinements for both data sets were carried out according to space groups $P4_132$ (No. 213) and $P2_13$ (No. 198). The difference between these symmetries leads to splitting of the 8c position of the former into two 4a positions for the latter, whereas the degradation of the 12d position of $P4_132$ to 12b in $P2_13$ increases the number of unconstrained positional parameters from one to three. The relations which convert the lower into the higher symmetric space group are $x_1 = 3/4 - x_2$ for the two 4a positions and $x = 1/8$, $y =$

* To whom correspondence should be addressed.

Table 1. Crystal and experimental data for LT $Au_{80-v}Cu_vSn_{20}$ with v = 45 and 60. When two sets of information separated by a semicolon are given, the first set refers consistently to the former composition.

Diffractometer	Nicolet *P*3/*F*; Syntex $P\bar{1}$
Radiation	Mo*K*α (λ = 71.069 pm)
Crystal system	Cubic
a/pm	676.2(2); 666.2(2)
V/pm³	3.092×10^8; 2.957×10^8
Space group	$P4_132$ (No. 213)
Crystal size/mm	0.04×0.05×0.06; 0.035×0.040×0.045
μ(Mo*K*α)/cm⁻¹	1086; 811
Scan mode	θ/2θ
Scan speed (2θ)/° min⁻¹	2.0; 1.0
Scan range (2θ)/°	2.4; 2.0
Maximum sin θ/λ/pm⁻¹	9.0×10^{-3}
Stability monitoring	3 Test reflections/ 100 observations
Observed reflections [$I>2.5\sigma(I)$]	167; 230
Weighting scheme	$w = [\sigma^2(F)]^{-1}$
No. of parameters refined	9
$R = \Sigma\|\|F_o\|-\|F_c\|\|/\Sigma\|F_o\|$	0.041; 0.051
$R_w = [\Sigma w(F_o-F_c)^2/\Sigma wF_o^2]^{1/2}$	0.032; 0.055
$S = [\Sigma w(F_o-F_c)^2/(n-m)]^{1/2}$	1.8; 4.7

variable and $z = 1/4 + y$ for the 12b position. The results of the refinements in terms of space group $P2_13$ showed that the above relations were satisfied within ~1.5 calculated standard deviations. Additional proof for space group $P4_132$ stems from the fact that only insignificant improvements in reliability factors and standard deviations were obtained on the introduction of the additional variables according to the lower symmetric space group. Hence, the space group choice was obvious, and there was no need to turn to criteria based on statistical model considerations.

Figures of merit are listed in Table 1, and final parameters are given in Table 2. Observed and calculated structure factors may be obtained from the authors upon request.

Discussion

A projection of the β-Mn-type crystal structure of LT $Au_{80-v}Cu_vSn_{20}$ is shown in Fig. 1, and interatomic distances are listed in Table 3. Several descriptions of this structure type occur in the literature. The early mistakes which had crept into Ref. 8 (in the report on Preston's[9] admirable structure determination of β-Mn from 1928) are thoroughly examined by Kripyakevich[10] and need not be dwelled on.

According to the more conventional coordination polyhedron description of the β-Mn-type structure by Kripyakevich[10] each *M*(I) atom is surrounded by 3 *M*(I) and 9 *M*(II) in a distorted icosahedral configuration, and each *M*(II) by 6 *M*(I) and 8 *M*(II) in a CN (coordination number) = 14 verticon arrangement. The latter is a very distorted, so-called Frank–Kasper[11] polyhedron like that found in the tetrahedral close-packed structures.[12] The location of one example of each kind of coordination polyhedron within the unit cell is shown in Figs. 1B and C. [It is also possible to identify empty $M(II)_6$ metaprisms; an intermediate between a trigonal prism and an octahedron – the latter designation being used by some authors.] The listings in Table 3 comply with such a centre-to-periphery atom description, whereas interatomic distances on the surfaces of the two kinds of coordination polyhedra are shown in Fig. 2. The numbering of the atoms in the illustrations should facilitate the identification of the centre-to-periphery interatomic distances according to Table 3. The two rather long centre-to-periphery *M*(II)–*M*(II) distances [350.5(1) and 345.1(1) pm in $Au_{35}Cu_{45}Sn_{20}$ and $Au_{20}Cu_{60}Sn_{20}$, respectively] in the CN = 14 verticon could mislead one to suspect that this assignment is incorrect, but these *M*(II) atoms indeed belong to the coordination shell according to the unique definition of CN by Frank and Kasper.[11] [Ref. 11 defines CN as the number of plane faces delimiting the domain of an atom in which the planes of this closed, innermost (Diriclet) polyhedron are equidistant between the atom in question and its neighbours.] The next, longer *M*(II)–*M*(II) distances (417.9 pm in Fig. 2B) are, however, just surface distances on the *M*(II) coordination polyhedron. The possibility that the coordination of *M*(II) is, in fact, CN = 16 rather than 14 has been checked for LT $Au_{80-v}Cu_vSn_{20}$. The outcome is that the normal plane bisecting the connection between II,11 (as the central atom) and II,1 in Fig. 1C just touches upon the domain of II,11 in one point, and II,1 is thus not a proper part of the coordination shell of II,11.

An alternative description of the β-Mn-type structure is provided by O'Keeffe and Andersson[13] in terms of a b.c.c. (body-centered cubic) packing of identical, non-intersecting rods along threefold axes (shown schematically in Fig. 3A). Each rod consists of a repeating sequence of $M(II)_6$ metaprisms and $M(I)M(II)_3$ tetrahedra (face or corner sharing) as shown in Fig. 3B. Fig. 3B refers to a repeating piece of one particular rod in the arrangement, the location of which is indicated in Fig. 3A (see also Fig. 1D). An $M(II)_6$ metaprism in one rod is corner-connected to six other metaprisms in adjacent rods; the 'notching' of the rods which run in different directions is neglected in Fig. 3A, but the tangled network of $M(II)_6$ metaprisms is depicted in Fig. 22 of Ref. 13.

A different rod-description of the β-Mn-type structure has recently been advanced by Nyman *et al.*[14] This approach considers the structure as built up of identical,

Table 2. Positional parameters and temperature factors for $Au_{35}Cu_{45}Sn_{20}$ and $Au_{20}Cu_{60}Sn_{20}$, with e.s.d.s in parentheses.[a]

	$Au_{35}Cu_{45}Sn_{20}$	$Au_{20}Cu_{60}Sn_{20}$
M(I)	x = 0.0629(3), U_{eq} = 0.72	x = 0.0643(2), U_{eq} = 1.25
M(II)	y = 0.2016(1), U_{eq} = 0.71	y = 0.2022(1), U_{eq} = 1.34

[a] *M*(I) refers to Cu in position 8c (x, x, x etc.) and *M*(II) to a statistical distribution of 0.583 Au + 0.083 Cu + 0.333 Sn and 0.333 Au + 0.333 Cu + 0.333 Sn for $Au_{35}Cu_{45}Sn_{20}$ and $Au_{20}Cu_{60}Sn_{20}$, respectively, in position 12d (1/8, y, 1/4 + y etc.). U_{eq} = 1/3 ΣU_{ii} in 10^6 pm².

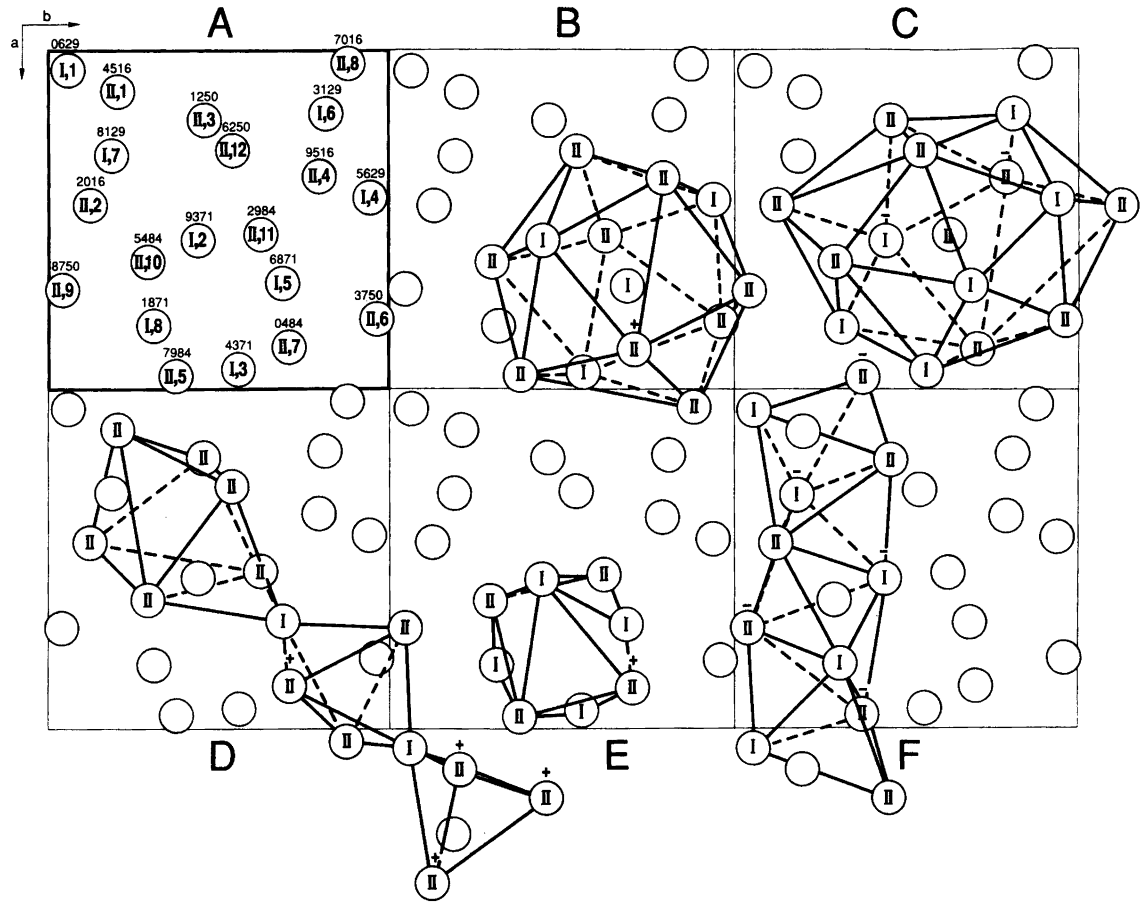

Fig. 1. (A) Projection of the β-Mn-type crystal structure. Numbers inside the atomic symbols (circles) give the kind of atom (roman numeral) and its identification number (arabic numeral) in the unit cell, this scheme being used in subsequent structural illustrations. Numbers outside the atomic symbols give the fraction ($\times 10^4$) of the projection axis for LT $Au_{80-v}Cu_vSn_{20}$, $v = 45$. (B) Location of one (distorted icosahedron) *M*(I) coordination polyhedron in the unit cell. (C) Location of one (CN = 14 verticon) *M*(II) coordination polyhedron in the unit cell. (D) Location of a rod built up of tetrahedra and metaprisms. (E) and (F) Location and orientation of a different kind of rod, build up of tetrahedra. Plus and minus refer to atoms in unit cells above and below, respectively.

'notched' (but otherwise non-intersecting) rods in a primitive cubic packing (shown schematically in Fig. 4A). These rods, which run parallel to the three cubic axes (coinciding with the symmetry element 4_1), consist entirely of face-sharing $M(I)_2M(II)_2$ tetrahedra (note that the two rod-descriptions make use of different tetrahedra). The inside

Table 3. Interatomic distances (in pm; < 400 pm, numbers in parentheses correspond to e.s.d.s in axes and positional parameters) in $Au_{35}Cu_{45}Sn_{20}$ and $Au_{20}Cu_{60}Sn_{20}$ in comparison with corresponding data for β-Mn and $Mn_{66}Ni_{20}Si_{14}$ according to Ref. 7.[a]

Distance		$Au_{35}Cu_{45}Sn_{20}$	$Au_{20}Cu_{60}Sn_{20}$	β-Mn	$Mn_{66}Ni_{20}Si_{14}$		Remarks
M(I)	–3 *M*(I)	253.4(3)	249.0(2)	236.4	235.3	235.3	I,5–I,2; I,3; I,4
	–3 *M*(II)	275.5(2)	272.5(2)	257.6	256.1	257.6	–II,7*; II,8*; II,9*
	–3 *M*(II)	282.2(2)	277.2(2)	263.4	262.6	262.4	–II,10; II,11; II,12
	–3 *M*(II)	286.7(2)	282.7(2)	268.0	267.8	266.6	–II,4; II,5; II,6
M(II)	–2 *M*(I)	275.5(2)	272.5(2)	257.6	256.1	257.6	II,11–I,2*; I,6
	–2 *M*(I)	282.2(2)	277.2(2)	263.4	262.6	262.4	–I,3; I,5
	–2 *M*(I)	286.7(2)	282.7(2)	268.0	267.8	266.6	–I,4; I,8
	–4 *M*(II)	282.9(1)	279.1(1)	264.6	263.4[b]	264.7[b]	–II,6; II,7; II,10; II,12
	–2 *M*(II)	287.2(1)	282.0(1)	267.2	265.3		–II,3; II,4*
	–2 *M*(II)	350.5(1)	345.1(1)	327.1	325.6		–II,2; II,2*

[a] *M*(I) and *M*(II) are explained in footnote to Table 2 as well as in the text. Note that *M*(I) is split into *M*(I,A) [Si mixed some Ni and/or Mn] and *M*(I,B) [Ni mixed with some Mn and/or Si] and that position *M*(II) is lower symmetric in the $AlAu_4$-type structure of $Mn_{66}Ni_{20}Si_{14}$. Roman and arabic numerals as well as asterisks in the remarks column specify distances according to Fig. 2.
[b] *M*(II)–2 *M*(II).

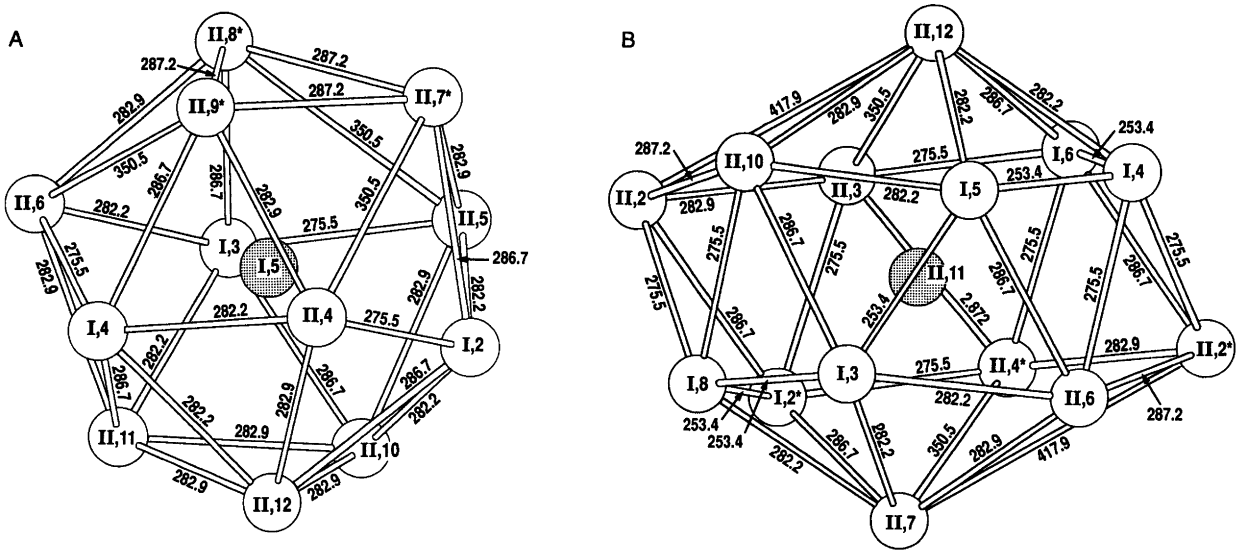

Fig. 2. Coordination polyhedra in the β-Mn-type crystal structure. (A) The M(I) icosahedron. (B) The M(II) CN = 14 verticon. Numbers inside the atomic symbols correspond to those in Fig. 1, asterisks mark identical atoms in another cell. Numbers outside the atomic symbols refer to interatomic distances on the surfaces of the two kinds of coordination polyhedra for $Au_{80-v}Cu_vSn_{20}$, v = 45. Centre-to-periphery interatomic distances are found in Table 3.

of one repeating piece of one particular rod is depicted in Fig. 4B (see also Figs. 1E, 1F and 4A). To secure translational repetition within the rods the tetrahedra have to be somewhat distorted, and the actual rods comprise two kinds of slightly different tetrahedra: these variants alternate in each rod. Adjacent, orthogonally oriented rods are united by sharing tetrahedral faces. The interstitial space between the rods in Fig. 4A consists of corner-connected metaprisms.

The three descriptions serve to put emphasis on different aspects of the β-Mn-type structure: (i) Kripyakevich's[10] approach focuses attention on the coordination situation of M(I) and M(II) and is suitable for bonding considerations. (ii) The angle of attack of O'Keeffe and Andersson[13] serves to stress that the b.c.c. rod packing concept rationalizes this

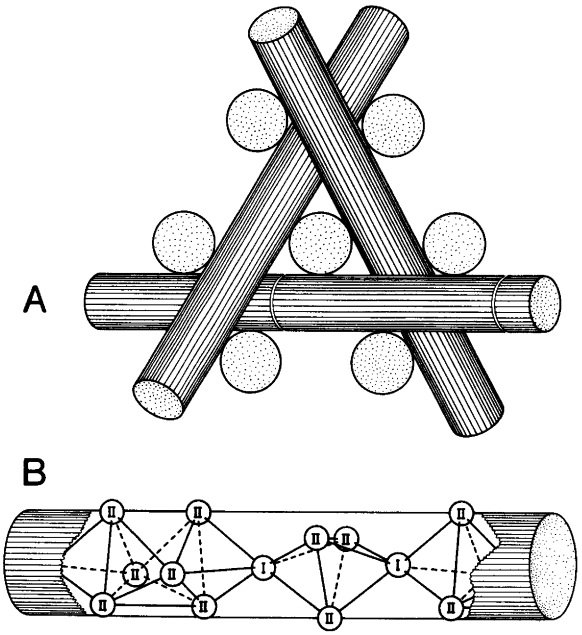

Fig. 3. (A) Schematic representation of extract of b.c.c. rod packing viewed along a threefold axis. 'Sawmarks' show the rod piece exposed in part B. (B) Succession of tetrahedra and metaprisms in one particular rod (see A) of the O'Keeffe–Andersson[13] representation of the β-Mn-type structure.

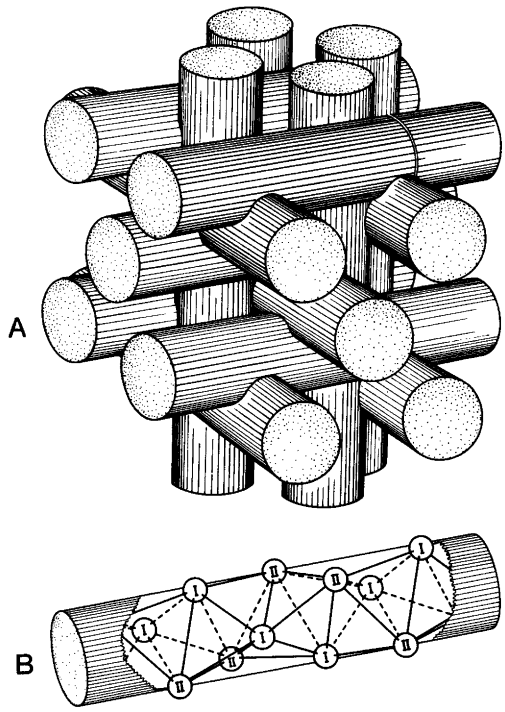

Fig. 4. (A) Schematic representation of extract of the primitive cubic rod packing model of Nyman *et al.*[14] for the β-Mn-type structure. 'Sawmark' shows the rod piece exposed in part B. (B) Succession of face-sharing tetrahedra within a piece of one particular rod (see A).

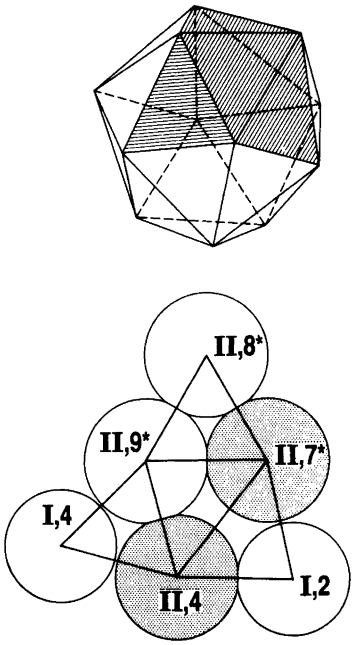

Fig. 5. Four neighbouring surface planes on the *M*(I) coordination polyhedron unfolded to a plane. Upper part of the illustration shows the location of the planes in question. Numbers inside the circles correspond to those in Fig. 2A. Relative size of circles is scaled to the CN = 12 radii[16] for LT $Au_{80-v}Cu_vSn_{20}$ = 45. Shading indicates *M*(II) atoms separated by interatomic distances of 350.5(1) and 345.1(1) pm for v = 45 and 60, respectively.

structure type as an efficient space filling type and is convenient to bring out relations to other structure types. (iii) The alternative rod picture of Nyman *et al.*[14] has similar advantages to that of O'Keeffe and Andersson, but carries the additional feature of connecting the distortions of the tetrahedral building elements to the space filling under the given structural symmetry.

In addition to LT $Au_{80-v}Cu_vSn_{20}$ reported here, Ref. 15 lists 38 phases with the β-Mn-type structure, of which 14 actually belong to a separate filled-up (sub-)class where the small non-metals B, C and N occupy the metaprismatic voids of the genuine structure type. Another four phases are listed under the $AlAu_4$ type, which represents a slightly distorted variant of the β-Mn type (*vide infra*).

Most of the phases with the β-Mn-type structure are unfortunately not well structurally characterized, but the handful (including the present examples) which are properly refined show remarkably little variation in the unconstrained positional parameters. The actual values of the parameters (for the present examples see Table 2) moreover nearly match the ideal values [$x = 1/(9 + \sqrt{33}) = 0.0678$; $y = (9 - \sqrt{33})/16 = 0.2035$][†] derived by O'Keeffe and Andersson,[13] but it is again appropriate to remind that this conclusion rest on a tiny selection of this structure family.

Another characteristic of the structure type concerned is the large number of centre-to-periphery distances involved in the coordination shell of *M*(I) and *M*(II) and their large scatter (Table 3). These characteristics have interesting consequences in relation to both the overall atomic arrangement as well as details thereof.

At first sight the reader may be surprised to learn that the percentage change in unit cell dimension on going from one β-Mn phase to another precisely matches the weighted average of the percentage changes in interatomic distances of the *M*(I) and *M*(II) coordination shells. The next reaction may be that this is only a rather trivial consequence of the approximate constancy of the positional parameters. However, the scatter in the individual values behind the weighted averages shows that this is indeed not the case, e.g., comparison of LT $Au_{80-v}Cu_vSn_{20}$ with v = 60 and 45 gives 1.10–1.84 % scatter (average 1.50 %), and between β-Mn and the two former 5.24–5.78 and 6.92–7.49 % scatter (averages 5.50 and 7.08 %), respectively. (Note that the average percentage values refer to relative changes and are hence not additive.) These gross structural relationships are therefore first and foremost a reflection of the fact that the *M*(I) and *M*(II) coordination shells contain a *representative selection* of the interatomic distances which build up the β-Mn-type unit cell.

If there were centre-to-periphery contacts between all atoms within both coordination shells and if the hard sphere model was satisfied, there should only occur three different 'bond' distances in the β-Mn-type structure, viz. *M*(I)–*M*(I), *M*(I)–*M*(II) and *M*(II)–*M*(II). Even if the strict rigidity of the atomic spheres is renounced, the significance of the two long centre-to-periphery *M*(II)–*M*(II) distances (Table 3) can be difficult to comprehend fully from, say, Figs. 1C and 2B. However, the origin of this long distance can e.g. be seen from the coordination shell of *M*(I) (Fig. 2A), since the *M*(I) and *M*(II) coordination polyhedra are interpenetrating. Fig. 5 shows four neighbouring surface planes on the icosahedron around *M*(I) unfolded to a plane, the relative size of the circles being scaled to the CN = 12 radii for LT $Au_{80-v}Cu_vSn_{20}$ for v = 45. The *M*(II)–*M*(II) distance in question, which here comes out between the shaded circles, is immediately seen to be a consequence of the packing of spheres of unequal size.

For the stipulation of estimated interatomic distances in LT $Au_{80-v}Cu_vSn_{20}$ an *effective* CN = 12 is accordingly used for both *M*(I) and *M*(II). The CN = 12 radii[16] for Au, Cu and Sn (for valence I, I and IV, respectively) give 255.6, 274.6 and 293.4 pm for the *M*(I)–*M*(I), *M*(I)–*M*(II) and *M*(II)–*M*(II) distances, respectively, in LT $Au_{35}Cu_{45}Sn_{20}$ and 255.6, 270.0 and 284.4 pm for the corresponding dis-

[†] The effective ideality criterion of O'Keeffe and Andersson requires that as many as possible of the shorter *M*(II)–*M*(II) distances and all the six shortest *M*(I)–*M*(II) distances are mutually equal. According to the numbering in Figs. 1 and 2, this can, e.g., be accomplished by constraining the distances II,2–II,1 to II,2–II,10 and I,5–II,10 to I,5–II,7*. This procedure leads to a quadratic equation for y and a linear connection between x and y. There is thus a second mathematical solution to this set of equations [$x = 1/(9 - \sqrt{33}) = 0.3072$, $y = (9 + \sqrt{33})/16 = 0.9215$], but this represents a crystallographic fake imposed by the use of the Pythagorean relation to express interatomic distances.

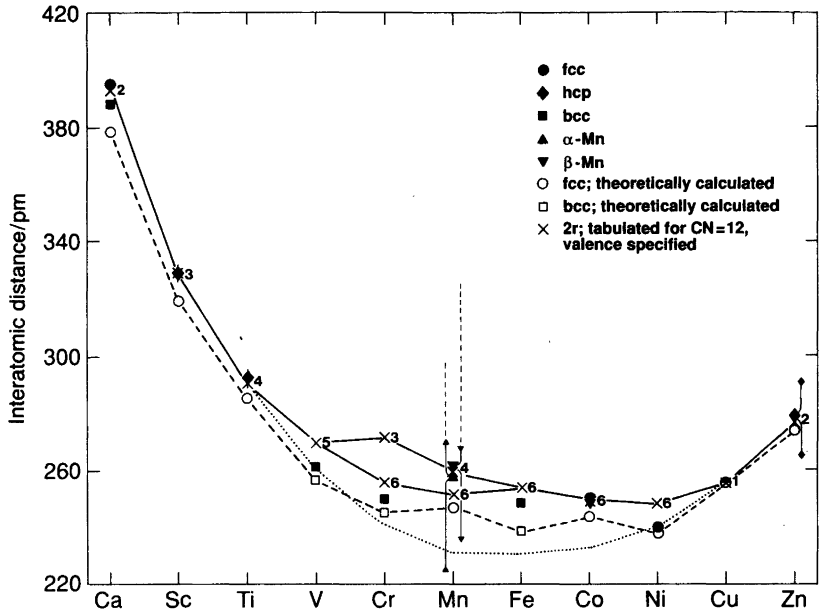

Fig. 6. Interatomic distances at 293 K for the elements Ca–Zn.[15] Legends to symbols are given on the illustration. Vertical bars give spread in interatomic distances when relevant, broken parts of the bars for manganese referring to elongated distances caused by the atomic arrangement (see text). Solid lines connect empirically assessed[16] distances, broken lines join theoretically calculated[19] (corrected for an assumed 1 % thermal expansion between 0 and 293 K and adjusted to 1 atm pressure) distances and dotted lines connect tentatively distances in 'low spin' Cr, Mn, Fe and Co.

tances in LT $Au_{20}Cu_{60}Sn_{20}$. Comparison of the observed values in Table 3 with these estimates shows deviations of −10.5 to 57.1 pm for LT $Au_{35}Cu_{45}Sn_{20}$ and −6.6 to 60.7 pm for LT $Au_{20}Cu_{60}Sn_{20}$, the largest discrepancies referring to the long *M*(II)–*M*(II) distance just considered. When the weighted averages within each distance category are considered, the mismatches between observed and estimated interatomic distances become −2.2, 7.0 and 7.5 pm for *M*(I)–*M*(I), *M*(I)–*M*(II) and *M*(II)–*M*(II), respectively, in LT $Au_{35}Cu_{45}Sn_{20}$, and similarly −6.6, 7.5 and 11.9 pm in LT $Au_{20}Cu_{60}Sn_{20}$. When the long *M*(II)–*M*(II) distance is excluded (from here on finally) the difference for the *M*(II)–*M*(II) category becomes −9.1 and −4.3 pm for $v = 45$ and 60, respectively.

A few remarks concerning the mismatches may be recorded. First, the distribution patterns of negative and positive discrepancies demonstrate a breakdown of the hard-sphere packing model. However, as partly seen from Fig. 5, rather limited amendments in shape from spheres to less symmetric bodies are needed to retain the essentials of the packing concept. Second, *M*(I) = Cu is smaller than tabulated in Ref. 16. Since Cu is the smallest of the three components, this finding can clearly not be accounted for as occurrence of some Au and/or Sn at the *M*(I) position, all the more because this possibility was already ruled out during the structure refinements. Third, the average size of *M*(I) and *M*(II) varies somewhat with the composition parameter v of LT $Au_{80-v}Cu_vSn_{20}$, that of *M*(I) = Cu decreasing and that of *M*(II) [= the mixture of Au, Cu and Sn] increasing with v. Some of these behaviours may in isolation be explained as a consequence of the geometrical arrangement of the β-Mn-type structure, but it is difficult to provide an entirely consistent explanation of all of them.

A few comments concerning the prototype β-Mn seem appropriate. Normally one obtains a relieving feeling of simplification on turning from intermetallic phases or compounds to pure elements. This is not the case for the crystal structure of LT $Au_{80-v}Cu_vSn_{20}$ versus β-Mn, where the challenge for the latter is to account for the large variation in interatomic distances (cf. Table 3) and more generally the need for two crystallographic positions in the structure of a metal. It is, e.g., easy to agree with Nesper[17] that 'the large differences in the bond lengths and the differing magnetic moments[18] indicate that these positions have different crystallochemical functions'. The statement refers specifically to α-Mn, but Nesper maintains that the two distinct positions in the β-Mn structure 'behave towards each other analogously to those in α-Mn'. However, the present authors disagree in the conclusion that 'this suggests that the majority components are cationic in nature and the minority components anionic'.

In order to rationalize the variation of the interatomic distances in α- and β-Mn, manganese should be seen as a part of a greater whole. Fig. 6 shows the variation of the interatomic distances in the crystal structures of the elements from Ca to Zn. Data[15] for different modifications are given when relevant; theoretically calculated[19] and empirically assessed[16] distances are included for comparison. Neglecting the relatively small systematic distinction between the observed and calculated data, the picture is unique in the beginning (Ca to Ti) and end (Cu and Zn) of the series. In the middle the situation is more ambiguous, and it reaches an apparent chaotic climax at Mn.

However, much of the mystery disappears when one remembers that a characteristic of the elements Cr, Mn, Fe and Co is their ability to take different electronic spin states. In turn, the electronic spin state influences the atomic size, and the dotted lines in Fig. 6 tentatively connect interatomic distances between 'low-spin' states of the said atoms.

Atoms with different electronic spin states on different crystallographic sites would indeed provide a simple, natural explanation of the large spread in interatomic distances in β- as well as α-Mn. As for the other members of the β-Mn-type family, the longest distance of the coordination shell is also for the prototype itself a structure-specific feature (*vide supra*). The formerly rather puzzling shortest distances are, on the other hand, merely a consequence of 'low spin' Mn in the sites concerned. This interpretation is consistent with the findings for the antiferromagnetic state of α-Mn,[18] whereas the lack of cooperative magnetism reported for β-Mn[18] should at best be regarded as indifferent to the picture. However, β-Mn has so far only been checked for conventional ferro- and antiferromagnetism, and the present authors strongly recommend a thorough re-examination for other, more exotic cooperative arrangements like heli-, cone- and fan-magnetism. There are indeed a number of other points in relation to Fig. 6 which could have been followed up, but we must now return to the central subject.

The distinction between the β-Mn and $AlAu_4$ structure types is connected with the space group alternatives $P4_132$ and $P2_13$ considered under the structure determinations for LT $Au_{80-\nu}Cu_\nu Sn_{20}$. There are in fact only two well documented examples for the $AlAu_4$-type structure, viz. the prototype[20,21] itself and $Mn_{66}Ni_{20}Sn_{14}$.[7] As seen from the comparison of $Au_{80-\nu}Cu_\nu Sn_{20}$ with β-Mn and $Mn_{66}Ni_{20}Si_{14}$ in Table 3, there appears to be little or nothing to be gained from the reduced symmetry for the latter phase from a solely crystallographic point of view. However, in combination with the chemistry the crystallographic formulae $Al_4Au_4Au_{12}$ and $(Si,Mn/Ni)_4(Ni,Mn/Si)_4Mn_{12}$ may indicate a reason for a separate $AlAu_4$-type branch on the β-Mn-type family tree.

A few comments concerning the structure in relation to the homogeneity range of LT $Au_{80-\nu}Cu_\nu Sn_{20}$ may also be appropriate. A noticeable fact is that the Au–Cu extension of the homogeneity range reported in Ref. 2, $\nu = 35$ (300 °C) and 69 (360 °C) does not have any special structural significance [crystallographic formulae $(Au_{0.125}Cu_{0.875})_8(Au_{0.667}Sn_{0.333})_{12}$ and $Cu_8(Au_{0.183}Cu_{0.483}Sn_{0.333})_{12}$, respectively]. However, as emphasized in Ref. 2, 'a phase diagram only shows the phases and phase fields that are most stable', and the above limits may therefore not deserve further speculation.

In Ref. 2 the $a(\nu)$ relationship for LT $Au_{80-\nu}Cu_\nu Sn_{20}$ was approximated by two linear sections with slightly different slopes. In view of the more detailed structure information provided by the present study, and in particular that the crossover point in Fig. 7 of Ref. 2 [$\nu = 55$; $Cu_8(Au_{0.416}Cu_{0.250}Sn_{0.333})_{12}$] has no special significance, it seems more reasonable to represent $a(\nu)$ by one slightly curved section. It is suggested that the curved shape of $a(\nu)$ reflects the effect of the internal pressure in the solid solution system, which gives Au a gradually reduced size as more of this larger component is introduced.

In relation to electron concentration considerations, LT and HT (high-temperature) $Au_{80-\nu}Cu_\nu Sn_{20}$ are intimately connected together, and a discussion is conveniently postponed to the forthcoming account on the γ-brass-type structure of the latter. Here we only record that the range of electron to atom ratios (1.54–1.62) for LT $Au_{80-\nu}Cu_\nu Sn_{20}$ balances on the edge of the stability range for the β-Mn-type structure according to the molecular orbital calculations of Hoistad and Lee.[22]

References

1. Karlsen, O. B., Kjekshus, A. and Røst, E. *Acta Chem. Scand. 44* (1990) 107.
2. Karlsen, O. B., Kjekshus, A. and Røst, E. *Acta Chem. Scand. 46* (1992) 197.
3. Karlsen, O. B., Kjekshus, A., Rømming, C. and Røst, E. *Acta Chem. Scand. 46* (1992) 442.
4. Gilmore, C. J. *J. Appl. Crystallogr. 17* (1984) 42.
5. Mallinson, P. R. and Muir, K. W. *J. Appl. Crystallogr. 18* (1985) 51.
6. Walker, N. and Stuart, D. *Acta Crystallogr., Sect. A 39* (1983) 158.
7. Shoemaker, C. B., Shoemaker, D. P., Hopkins, T. E. and Yindepit, S. *Acta Crystallogr., Sect. B 34* (1978) 3573.
8. *Strukturbericht,* Band II, 1928–1932, p. 3.
9. Preston, G. D. *Phil. Mag. 5* (1928) 1207.
10. Kripyakevich, P. I. *Kristallografiya 5* (1960) 273; transl. *Sov. Phys. Crystallogr. 5* (1960) 253.
11. Frank, F. C. and Kasper, J. S. *Acta Crystallogr. 11* (1958) 184.
12. Shoemaker, C. B. and Shoemaker, D. P. *Monatsh. Chem. 102* (1971) 1643.
13. O'Keeffe, M. and Andersson, S. *Acta Crystallogr., Sect. A 33* (1977) 914.
14. Nyman, H., Carroll, C. E. and Hyde, B. G. *Z. Kristallogr. 196* (1991) 39.
15. Villars, P. and Calvert, L. D. *Pearson's Handbook of Crystallographic Data for Intermetallic Phases,* Vols. 1–3, American Society for Metals, Metals Park, OH 1985.
16. Teatum, E., Gschneidner, K. and Waber, J. *Compilation of Calculated Data Useful in Predicting Metallugical Behavior of the Elements in Binary Alloy Systems,* LA-2345, U.S. Department of Commerce, Washington, DC 1960; see also Pearson, W. B. *The Crystal Chemistry and Physics of Metals and Alloys,* Wiley-Interscience, New York 1972.
17. Nesper, R. *Angew. Chem., Int. Ed. Engl. 30* (1991) 789.
18. Kasper, J. S. and Roberts, B. W. *Phys. Rev. 101* (1956) 537.
19. Moruzzi, V. L., Janak, J. F. and Williams, A. R. *Calculated Electronic Properties of Metals,* Pergamon, New York 1978.
20. Ullner, O. E. *Arkiv. Kemi. Min. Geol. 14A* (1940) No. 3, 1.
21. Büchler, H. and Range, K.-J. *J. Less-Common Met. 161* (1990) 347.
22. Hoistad, L. M. and Lee, S. *J. Am. Chem. Soc. 113* (1991) 8216.

Received April 14, 1992.